THE JOURNAL OF PHYSICAL CHEMISTRY B

ARTICLE

pubs.acs.org/JPCB

FRET-Based Ratiometric Detection System for Mercury Ions in Water with Polymeric Particles as Scaffolds

Chao Ma, Fang Zeng,* Lifang Huang, and Shuizhu Wu*

College of Materials Science & Engineering, South China University of Technology, Guangzhou 510640, China

Supporting Information

ABSTRACT: Mercury pollution is a global problem, and the development of stable and sensitive fluorescent probes for mercury ions in the water phase has long been sought. In this work, a novel fluorescence resonance energy transfer (FRET)-based ratiometric sensor for detecting Hg^{2+} in pure water was demonstrated. Polymeric nanoparticles prepared by miniemulsion polymerization of methyl methacrylate and acrylic acid were used as the scaffold for the FRET-based sensor. A hydrophobic fluorescent dye nitrobenzoxadiazolyl derivative (NBD) was embedded in the nanoparticles during the polymerization and used as the donor. A spirolactam rhodamine derivative SRHB−NH_2 was synthesized and then covalently linked onto the particle surface and used as an ion recognition element. The presence of Hg^{2+} in the water dispersion of nanoparticles induced the ring-opening reaction of the spirolactam rhodamine moieties and led to the occurrence of the FRET process, affording the nanoparticle system a ratiometric sensor for Hg^{2+}. The nanoparticle sensor can selectively detect the Hg^{2+} in water with the detection limit of 100 nM (ca. 20 ppb). It has been found that the FRET-based system with smaller nanoparticles as the scaffold exhibited higher energy transfer efficiency and was more preferred for the accurate ratiometric detection. Moreover, the FRET-based sensor was applicable in a relatively wide pH range (pH 4−8) in water; thus, this approach may provide a new strategy for ratiometric detection of analytes in environmental and biological applications.

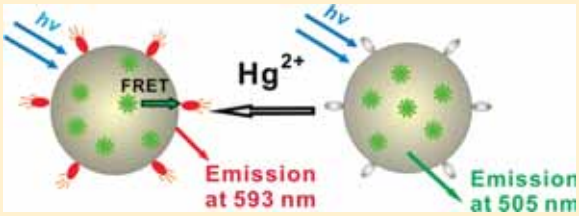

1. INTRODUCTION

Mercury pollution is a global problem because of its deleterious effects on human health and the environment.[1−4] The dangerous problems have promoted the development of detecting mercury ions.[5−8] In recent years, fluorescence spectroscopy has become a powerful tool for detecting transition and heavy metal ions in ultratrace quantity, due to its sensitivity and simplicity.[9,10] Thus, the design and development of fluorescent probes for Hg^{2+} has attracted a great deal of attention. To date, a number of fluorescent sensors for Hg^{2+} ions have been reported,[9−15] which are capable of detecting Hg^{2+} ions by fluorescence enhancement or quenching. However, many of the chemosensors have only one signal for detecting, i.e., the fluorescence intensity, and the environmental and instrumental conditions will affect the detection result. Ratiometric chemosensors can eliminate or reduce the effects of these factors by the self-calibration of the two emission bands.[16−27] Unlike those one-signal sensors, the ratiometric fluorescence sensors contain two different chromophores and use the ratio of the two fluorescence intensities to quantitatively detect the analytes, and they can eliminate most ambiguities in the detection by self-calibration of two emission bands; thus, some external factors such as excitation source fluctuations and sensor concentration will not affect the ratio between the two fluorescence intensities.[16−19] Recently, some ratiometric fluorescence sensors have already been developed, including the spriolactam rhodamine derivatives sensors.[16,20−27] However, many of these sensors can only work in the organic or mixed solvents, which cannot be directly used in environmental and biological systems. Thus, designing water-soluble (dispersible) chemosensors is of great importance.

Recently, the fluorescence resonance energy transfer (FRET), which involves the nonradiative transfer of excitation energy from an excited donor to a proximal ground-state acceptor,[28−32] has been employed to design ratiometric sensors.[25,26,33−37] The FRET-based sensors can be designed in the form of a small molecule, which contains two fluorophores connected by a spacer through covalent links.[25−27] The small molecule sensors usually exhibit high sensitivity for detecting analytes; however, some of them are indissolvable in water, and some chromophores (donor or acceptor) in these sensors tend to aggregate to form dimers, trimers, and some other aggregates in water due to the $\pi-\pi$ interactions between the chromophores.

On the other hand, the FRET systems can also be built within the particles, such as quantum dots,[33−49] silica,[50−52] and polymer particles;[53−66] these water-dispersible particles with different dyes usually exhibit high fluorescence brightness and photostability

Received: October 6, 2010
Revised: December 6, 2010
Published: January 20, 2011

in water. According to the Förster's energy transfer theory,[28,67] the FRET process can take place between a donor and an acceptor within a distance in the $R_0 \pm 50\%$ R_0 range, where R_0 is the Förster critical distance. Generally, the distance between the donor and the acceptor should be within the range of 1−10 nm. To design a sensing system for detecting ions with the particles as the scaffold, the probe (ion recognition element) should be placed on the surface of the particles to enhance the interaction between the ions and the recognition element, and the donor dye should be embedded into the particles for protection. Thus, to design the FRET-based detection system with high sensitivity, the control over the distance between the donor and probe (precursor of the acceptor) in individual particles is one major task. For quantum dots, metallic and silica particles, their sizes can be readily controlled to very small values to ensure higher energy transfer efficiency and higher detection sensitivity. For the polymer particles, which possess versatile structural design and functionalization capability, making them small in size and applicable as the FRET scaffold by conventional emulsion polymerization is not an easy task. To address this issue, Larpent and co-workers[55] prepared nanosized fluorescent polymer particles (15 nm diameter) via microemulsion and obtained a FRET-based "turn-off" sensor for Cu^{2+}. On the other hand, by adopting a grafting reaction with *tert*-butyl hydroperoxide as the initiator, our group constructed a FRET system within the amphiphilic core/shell polymer nanoparticles with polyethylene imine (PEI) as the shell;[56] nonetheless, the abundant amino groups on the nanoparticle surface will definitely interfere with the metal ion detection. As for the fabrication of the polymeric particle-based ratiometric ion sensor, recently we incorporated both the donor dye and the probe into amphiphilic diblock copolymer micelles and formed a FRET-based ratiometric sensor for copper ions in water;[57] however, this kind of ratiometric sensor may face dye leakage caused by dilution or temperature variation due to the instability of the micelles. To our best knowledge, so far, there is no other report on the use of polymeric particles as the scaffold for the FRET-based ratiometric ion sensor.

The recently developed miniemulsion technology provides a promising method to address this problem. Miniemulsions are aqueous dispersions of relatively stable and small (40−500 nm) oil (oil-soluble monomer) droplets prepared by using high-force dispersion devices.[68−70] In the whole miniemulsion polymerization process, there may be little or no micellar or homogeneous nucleation. Thus, each of the droplets can be regarded as an individual batch reactor, and a variety of substances can be introduced into individual miniemulsions and then be subject to polymerization to obtain colloidal particles.[71−77] Landfester et al. incorporated the magnetic nanoparticles and fluorescent dyes into polymeric nanobeads via miniemulsion polymerization and obtained fluorescent and magnetic dual report nanoparticles usable in biomedical fields.[71] Kawaguchi et al. prepared highly fluorescent polymer particles with Eu(III) beta-diketonates complex as a fluorophore by miniemulsion polymerization technique.[74] In view of the advantages of the miniemulsion polymerization, we suppose miniemulsion polymerization might turn out to be a facile method for incorporating the donor into nanoparticle and keeping the particle size relatively small without introducing large amount of surfactant.

Herein, we report a new strategy for constructing a FRET-based ratiometric chemosensor for Hg^{2+} detection in water by using polymeric nanoparticles as the scaffold. In this study, the

Scheme 1. Formation of a FRET-Based System with Polymeric Nanoparticle as the Scaffold and Its Application as Ratiometric Fluorescence Sensor for Mercury Ion in Water [a]

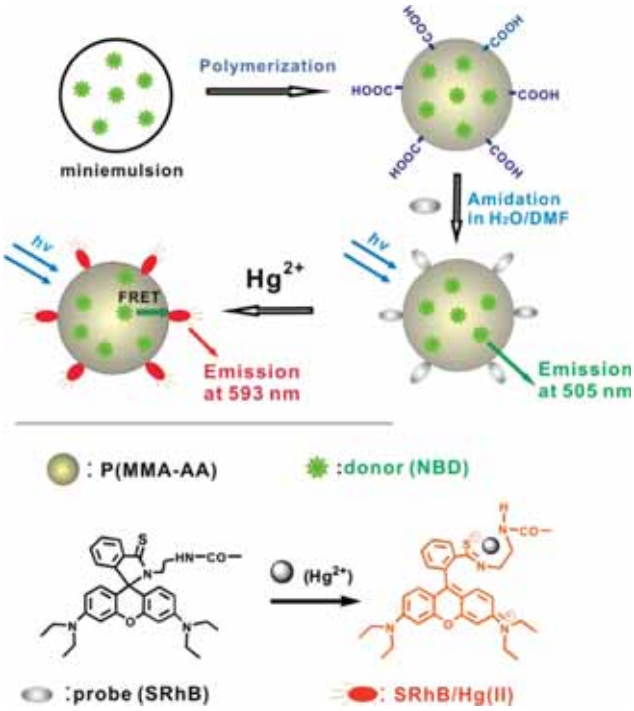

[a] On the particle surface, the surfactant molecules are not shown.

nanosized polymer particles were prepared via miniemulsion polymerization to embed a hydrophobic dye nitrobenzoxadiazolyl (NBD) into the hydrophobic core as the FRET donor. The Hg^{2+} ion probe, a spirolactam rhodamine derivative which is water-insoluble, was then covalently linked to the particle surface via the amidation reaction in water/DMF mixture. For this nanoparticle-based sensing system, the presence of Hg^{2+} can induce an efficient ring-opening reaction of the spirolactam rhodamine. Upon blue light irradiation, the excited-state energy of the donor NBD in the particle cores can be transferred to the ring-opened rhodamine derivative on the particle surface, realizing the FRET-based ratiometric detection for mercury ions in water, as shown in Scheme 1. For this approach, a much lesser amount of surfactant was used in nanoparticle preparation than that in microemulsion polymerization (generally, the surfactants account for over 10 wt % of the monomer amount in microemulsion polymerization), and this may reduce the inference of the surfactant molecules on the binding of the probe and the analytes; moreover, the distributions of fluorescent dyes inside the nanoparticles are much more uniform than those in the particles prepared via heterogeneous nucleation emulsion polymerization.

2. EXPERIMENTAL SECTION

2.1. Materials. Rhodamine B, 1,2-ethylenediamine, Lawesson's reagent, HEPES sodium salt, *N*-(3-dimethylaminopropyl)-*N*′-ethylcarbodiimide hydrochloride (EDC), ethylene glycol dimethacrylate, *N*-hydroxysuccinimide (NHS), and hexadecane (HD) were obtained from Alfa Aesor. Sodium dodecyl sulfate (SDS), potassium persulfate, chloride salts of metal ions

(K^+, Na^+, Ca^{2+}, Mg^{2+}, Al^{3+}, Zn^{2+}, Fe^{3+}, Mn^{2+}, Pb^{2+}, Cu^{2+}, Co^{2+}, Ni^{2+}, Cr^{3+}, and Hg^{2+}), and $AgNO_3$ were obtained from Aldrich. Methyl methacrylate (MMA), acrylic acid (AA), triethylamine, methanol, *N*,*N*-dimethylformamide (DMF), and toluene were analytically pure regents and repurified before use.

2.2. Preparation of Donor-Containing Nanoparticles. The fluorescence dye NBD was synthesized according to our previously reported procedure.[60] Then, the miniemulsion polymerization was employed to prepare the NBD-doped nanoparticles. For a typical run, NBD was mixed with methyl methacrylate (MMA, 2.5 g), acrylic acid (AA, 0.1 g), ethylene glycol dimethacrylate (EDMA, 0.1 g), and hexadecane (HD, 0.3 g), and the mixture was dispersed into water with surfactant sodium dodecyl sulfate (SDS, 0.13 g). After that, the dispersion was subject to 420 W ultrasonic wave for 20 min. The initiator potassium persulfate (KPS, 0.1 g) was then added into the monomer mixture to initiate the miniemusion polymerization at 60 °C. Finally, a stable and translucent dispersion of NBD-containing nanoparticles with the particle diameter of 40 nm was thus obtained.

2.3. Synthesis of Amino-Containing Mercury Ion Recognition Probe (SRHB−NH_2). First, a spirolactam Rhodamine B derivative (RHB−NH_2) was synthesized according to the literature.[78] Rhodamine B (5 g, 10.4 mmol) was dissolved in 100 mL of hot methanol, followed by the addition of ethylenediamine (200 mmol). The reaction mixture was refluxed for 20 h until the fluorescence of the solution disappeared. After cooling to room temperature, the solvent was evaporated under vacuum. CH_2Cl_2 (150 mL) and water (300 mL) were added, and the organic layer was separated, washed with water several times, and dried over anhydrous sodium sulfate. After filtration of sodium sulfate, the solvent was removed under reduced pressure. Then the resulting solid was purified by column chromatography with ethyl acetate/petroleum ether (volume ratio 3:1) to give the RHB−NH_2 in 78% yield. ^{1}H NMR spectrum of SRHB−NH_2 ($CDCl_3$, 400 MHz) δ: 7.89−7.87 (m, 1H), 7.45−7.42 (m, 2H), 7.09−7.07 (m, 1H), 6.44−6.36 (m, 4H), 6.28−6.25 (m, 2H), 3.36−3.29 (t, 8H), 3.21−3.17 (t, 2H), 2.44−2.39 (t, 2H), 1.18−1.14 (t, 12H). ESI m/z $[M + H]^+$ = 485.6.

Afterward, to synthesize the mercury ion recognition probe, the RHB−NH_2 (485 mg, 1 mmol) and Lawesson' reagent (404 mg, 1 mmol) were dissolved in dry toluene, and the mixture was refluxed for 6 h under N_2 atmosphere; after removal of toluene, the residue was dissolved in dichloromethane and purified by column chromatography with ethyl acetate/petroleum ether (volume ratio 1:3) as eluent to afford the mercury ion recognition probe SRHB−NH_2 in 15% yield (shown in Supporting Information Scheme S1). ^{1}H NMR spectrum of SRHB−NH_2 ($CDCl_3$, 400 MHz) δ: 8.16−8.14 (m, 1H), 7.49−7.427 (m, 2H), 7.12−7.09 (m, 1H), 6.42−6.35 (m, 4H), 6.28−6.26 (m, 2H), 3.62−3.58 (t, 2H), 3.36−3.28 (t, 8H), 2.53−2.50 (t, 2H), 1.20−1.16 (t, 12H). ESI m/z $[M + H]^+$ = 501.5.

2.4. Grafting Mercury Ion Probe SRHB−NH_2 onto Particle Surface. The NBD-containing nanoparticle dispersion (5 mL) was diluted to a concentration of 125 mg/L (1.25 wt %). Then, EDC (8 mg, 0.042 mmol) and NHS (4.8 mg, 0.042 mmol) were added into the solution under the mild stirring. The reaction was continued for 3 h at room temperature at pH 6.0. After that, DMF (1 mL) was added into the system. SRHB−NH_2 (5 mg, 0.01 mmol) was dissolved in DMF (2.5 mL) and added dropwise over 1 h at pH 8.0. Additional water was added in the system to maintain the ratio of the water/DMF at about 1:10 during the process. The solution was stirred for 3 h at room temperature. The excess reactants were removed by filtration and dialysis, and the dispersions were diluted to 50 mL. Finally, a stable dispersion of NBD-containing nanoparticles with SRHB on their surfaces was obtained (Scheme S1 in the Supporting Information).

2.5. Characterization. ^{1}H NMR spectra were recorded on a Bruker Avance 400 MHz NMR spectrometer. The mass spectrum was obtained through a Bruker Esquire HCT Plus mass spectrometer. The sizes of nanoparticles were measured in solution using dynamic light scattering (DLS) on a Malvern Nano-ZS90 particle size analyzer and in the dry state by atomic force microscopy (AFM, Seiko SII 400). UV−vis spectra were obtained on a Hitachi U-3010 UV−vis spectrophotometer. The static and time-resolved fluorescence spectra were recorded on a Hitachi F-4600 fluorescence spectrophotometer and an Edinburgh FL920 fluorescence spectrophotometer, respectively, and all the static and time-resolved fluorescence measurements were conducted under air (in the presence of oxygen). TEM images for the nanoparticles were obtained on a JEM-100CXII transmission electron microscope (TEM) at 60 kV, and the negative staining method using phosphotungstic acid was employed to outline the PMMA-based nanoparticles.

3. RESULTS AND DISCUSSION

3.1. Synthesis of Fluorophores. The donor dye NBD was synthesized via the reaction of 4-chloro-7-nitrobenzofurazan (NBD−Cl) with fatty amine according to our previously reported method.[60] The mercury ion recognition element (precursor of the acceptor) SRHB−NH_2 was synthesized via a two-step reaction as shown in Scheme S1. First, RHB-NH_2 was obtained from the reaction of rhodamine B with 1,2-ethylenediamine; then, the Lawesson's reagent was used to replace the oxygen atom on the carbonyl group in RHB−NH_2 with sulfur atom, forming a mercury ion recognition probe. The synthesized fluorophores were characterized by NMR and MS as shown in Figures S1−S5.

3.2. Preparation of Nanoparticles with NBD Dye in Their Cores. The NBD-containing nanoparticle dispersion was prepared via miniemulsion polymerization. In this study, two nanoparticle samples with their average diameter of 40.7 nm (sample NP40) and 60.2 nm (NP60) were obtained by adjusting the amount of surfactant, monomer concentration in water, as well as the ultrasonification power and time. The fluorophore NBD was embedded in the nanoparticles during the polymerization and would serve as the FRET donor in the subsequent detection process. The absorption spectra and emission spectra of NBD-containing nanoparticles are shown in Figure 1. As a hydrophobic dye, NBD has a very low solubility in pure water and shows a weak adsorption and fluorescence emission. However, upon being introduced into the nanoparticles, NBD shows a prominent absorption and fluorescence emission as it was located in a low-polarity circumstance. The amount of the NBD in the nanoparticle dispersion can be deduced by using the absorbance values assuming that the molar extinction coefficient of NBD in nanoparticles is the same as that in a certain organic solution.[54,57]

3.3. Grafting Mercury Ion Recognition Probe SRHB−NH_2 onto the Nanoparticle Surface. A FRET-based ratiometric sensor requires two different fluorophores to form the donor and the acceptor. In this study, we synthesized a spirolactam rhodamine with an amino end group (SRHB−NH_2) as the mercury

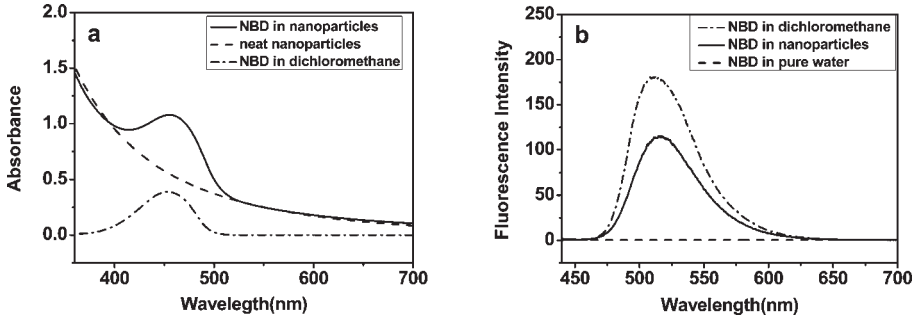

Figure 1. Absorbance (a) and emission (b) spectra of NBD dye in different environments (under air atmosphere).

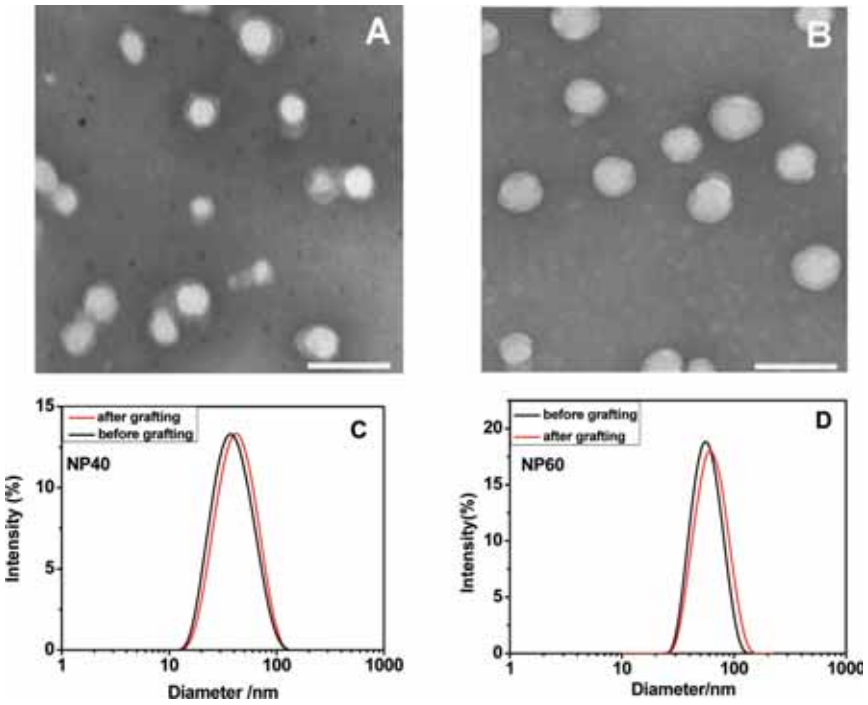

Figure 2. (A, B) TEM image for samples NP40 and NP 60, respectively (after grafting). The negative staining method using phosphotungstic acid was employed to outline the PMMA-based nanoparticles. Scale bar: 100 nm. (C, D) Particle size distribution for samples NP40 and NP60, respectively, determined by DLS before and after grafting the Hg^{2+} recognition probe. The average diameter for the two samples after grafting is 40.7 nm (NP40) and 60.2 nm (NP60), respectively.

ion recognition probe and then covalently linked the dye onto the nanoparticle surface through an amidation reaction between the amino groups on the probes and the carboxyl groups on the nanoparticle surface. However, SRHB−NH_2 is hardly soluble in pure water; thus, we used water/DMF mixture as the reaction medium for the amidation reaction, and DMF was removed through dialysis after the reaction. The particle size distributions for the samples before and after grafting are shown in Figure 2, and the AFM image for sample NP40 after grafting is shown in Figure S6 in the Supporting Information.

Figure 3 shows the absorption spectra of NP40 nanoparticle dispersion upon addition of mercury ions at pH 7.0 (HEPES). Before addition of Hg^{2+}, there is only one absorption profile of NBD at about 450 nm (as shown in Figure 1a), while addition of Hg^{2+} led to a new absorption band at about 570 nm. This proves that the addition of Hg^{2+} can cause the probe to change its structure from the spirolactam state to the ring-opened state.

3.4. Ratiometric Fluorescence Sensing of Hg^{2+} in Water.

We measured the fluorescence changes of the particle-based system upon addition of Hg^{2+} ion in HEPES buffer dispersion and established a working curve by plotting the ratio of the emission intensities at 593 and 505 nm (I_{593}/I_{505}) versus mercury ion concentration, as shown in Figure 4. Figure 4a shows the fluorescence spectra of the nanoparticle dispersion with the addition of Hg^{2+}. It can be seen that in the absence of Hg^{2+} ion, excitation of the nanoparticle dispersion at 420 nm resulted in the emission profile of the NBD at around 505 nm ($\Phi = 0.9$). With the addition of Hg^{2+} ions, the NBD's emission at 505 nm gradually decreased, and a new emission band at 593 nm appeared, which corresponded to the fluorescence emission of rhodamine B (the open-ring state). In the presence of Hg^{2+}, the spirolactam rhodamine group changed into the ring-opened state due to its complexation with Hg^{2+}. Meanwhile, the fluorescence of the nanoparticle dispersion also

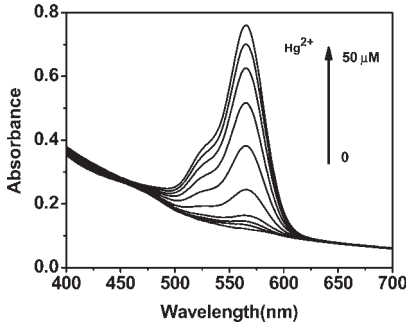

Figure 3. Absorption spectra of a nanoparticle-based sensor upon addition of Hg^{2+} (HEPES, pH 7.0). (Sample NP40, the concentration for NBD and the probe in the dispersion is 1.54×10^{-6} and 6.09×10^{-5} mol/L, respectively.)

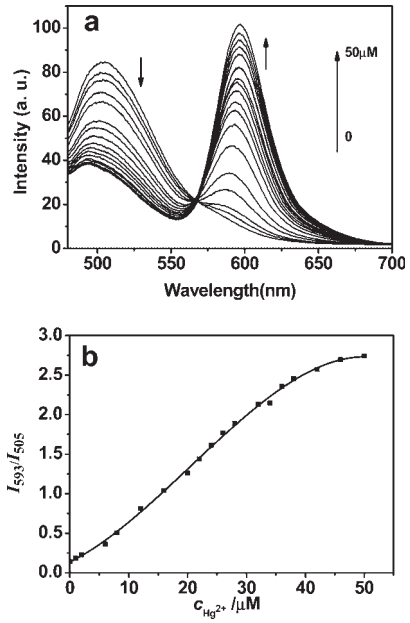

Figure 4. (a) Fluorescence spectra (λ_{exc}, 420 nm; slit, 5 nm/5 nm) of the nanoparticle dispersion of NP40 (NBD, 1.54×10^{-6} M; SRHB, 6.09×10^{-5} M) upon titration of Hg^{2+}. (b) Ratio of the fluorescence intensity of NBD to that of rhodamine B (I_{593}/I_{505}) for the nanoparticle dispersion upon addition of Hg^{2+}, (pH = 7.0, HEPES buffered water). The data was fitted with the equation $y = 0.135 + (3.68 \times 10^{-2})x + (1.64 \times 10^{-3})x^2 - (2.68 \times 10^{-5})x^3$. The fluorescence spectra were measured under air atmosphere.

changed from green to red upon addition of Hg^{2+} (Figure S7). Figure 4b presents the relationship between Hg^{2+} concentration and the ratio of the fluorescence intensities at 593 and 505 nm (I_{593}/I_{505}), and a three-order polynomial equation was used to fit the data. As the Hg^{2+} concentration is below 35 μM, the I_{593}/I_{505} value increases steadily with the increasing concentration of the added mercury ions; when the Hg^{2+} concentration is higher than 35 μM, the I_{593}/I_{505} increases slowly with the increasing concentration of Hg^{2+}, and finally the curve of I_{593}/I_{505} vs $C_{Hg(II)}$ levels off. This result indicates the nanoparticle-based system can serve as a reliable ratiometric fluorescent sensor for Hg^{2+} in water as the Hg^{2+} concentration is below 35 μM. It is likely that the FRET process was switched on by Hg^{2+} ions as excitation of

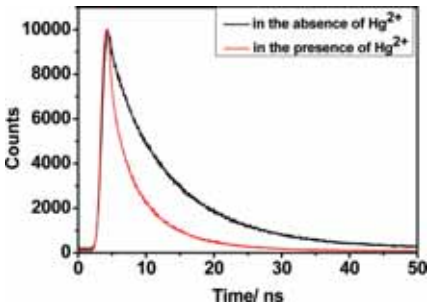

Figure 5. Fluorescence decay curves recorded for NBD in a nanoparticle dispersion (sample NP40, in pH 7.0 HEPES buffer solution). Black curve: in the absence of Hg^{2+}. Red curve: in the presence of Hg^{2+} (5×10^{-5} M). The decay curves were recorded under air atmosphere.

the NBD at 420 nm resulted in the emission of rhodamine B with a maximum of 593 nm. This detection system has two separated emission bands with comparable intensities, which ensures accuracy in determining their intensities and ratios. By adjusting the concentration of the dyes within the particle dispersion, the detection limit of a nanoparticle-based system can reach 100 nM (or 20 ppb), as shown in Figure S9.

The overlap of the emission spectra of NBD and absorption spectra of ring-opened rhodamine (Figure S8) also suggests that the two fluorophores constitute a donor−acceptor pair of an energy transfer system; To further prove the occurrence of energy transfer from the excited state of NBD to the probe/Hg^{2+} complex, we recorded the decay curves for NBD in the nanoparticle dispersion before and after adding mercury ions into the dispersion, as shown in Figure 5. In this polymeric particle system, with the absence of mercury ions, there is no FRET involved, and we can obtain an intensity decay curve for the donor, from which a decay time (or lifetime) was determined as 9.7 ns by fitting the data to a single exponential decay curve. On the other hand, with the addition of mercury ions, the FRET process take place upon exciting the donor. In consideration of the complexity of the polymeric particle-based FRET system in which one donor (or acceptor) may interact with multiple acceptors (or donors), and the separation distance between the donors and the acceptors is not a single value, we calculated the average decay time $\langle t \rangle$ (5.7 ns) by averaging t over the intensity decay of the donor using a numerical integration software according to eq 1 and used it as the apparent lifetime for the donor upon addition of mercury ions.

$$\langle t \rangle = \frac{\int_{t1}^{t2} tI(t)\,dt}{\int_{t1}^{t2} I(t)\,dt} \quad (1)$$

where $I(t)$ is the time-dependent intensity for the donor, t_1 is the time at which the intensity began to decay, and t_2 is the time at which the integration ends (30 ns in this study).

The apparent lifetime calculated according to eq 1 is shorter than the lifetime for the donor in the absence of mercury ions, and the decrease in fluorescence emission lifetime of the donor upon addition of mercury ions provides additional evidence that in this system the FRET process was turned on by mercury ion. As for the contribution of the photoinduced electron (or charge) transfer (PET) to the quenching of the donor's fluorescence, we think that it is not possible in the current case, because the donors are placed inside the hydrophobic PMMA cores of the polymeric

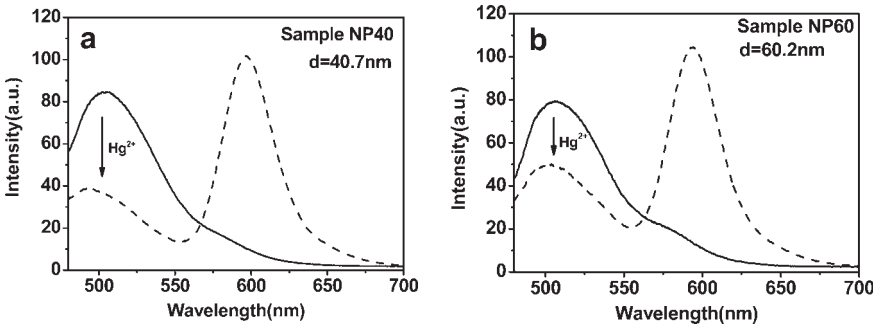

Figure 6. Maximum fluorescence intensity change for NBD (donor) upon addition of Hg^{2+} for two nanoparticle samples with the average diameter of 40.7 nm (a) and 60.2 nm (b), respectively. Solid curves: in the absence of mercury ion. Dashed curves: in the presence of excessive amount (50 μM) of mercury ions.

Table 1. Comparison of Experimental Energy Transfer Efficiency and Effective Energy Transfer Volume for Two Nanoparticle Samples

sample	diameter (nm)[a]	E_m[b] (%)	V_e[c] (%)
NP40	40.7 ± 0.7	57.6 ± 0.6	53.8 ± 0.5
NP60	60.2 ± 0.9	38.5 ± 0.5	39.3 ± 0.4

[a] Particle diameters determined by light-scattering method based on five measurements. [b] $E_m = 1 - I_{Hg}/I_0$, e.g., the experimental (measured) energy transfer efficiency based on three measurements, I_0—fluorescence intensity of NBD (at 505 nm) in the absence of mercury ions, I_{Hg}—fluorescence intensity of NBD (at 505 nm) in the presence of excessive amount (50 μM) of mercury ions. [c] V_e, the fraction of effective energy transfer volume in overall particle volume, as illustrated in Scheme S2.

particles, and the electrons (if any) cannot migrate through the low-polar and nonconductive PMMA medium.

Figure 6 shows the maximum fluorescence change of the donor NBD upon addition of mercury ions for two nanoparticle samples with different diameters. For this experiment, an excessive amount of Hg^{2+} has been added into the dispersions so as to quench the NBD emission as much as possible; thus, we can obtain the experimental energy transfer efficiency E_m for the nanoparticle systems, and the measured E_m values for sample NP40 and NP60 are shown in Table 1.

Unlike some FRET-based small molecular chemosensors in which donor and acceptor are connected by covalent bonds, the two fluorophores in the nanoparticles of the current work were segregated, with the donor dispersed in the nanoparticle core and the acceptor connected on the surface of the particle. The distance between the donor and acceptor moieties within the nanoparticles is not a fixed value and cannot be accurately determined, and one donor can interact with multiple acceptors residing in close proximity simultaneously. According to the Förster nonradiative energy transfer theory,[37,67] the energy transfer efficiency E, expressed by eq 2, depends on the Förster critical radius R_0, the average number of acceptors (ring-opened rhodamine B/Hg^{2+} complex) interacting with the donor n, and the distance (r) between the donor (NBD) and the acceptor. The energy transfer is effective over distances in the $R_0 = \pm 50\%$ R_0 range.

$$E = \frac{nR_0^6}{nR_0^6 + r^6} \quad (2)$$

The magnitude of R_0 is dependent on the spectral properties of the donor and the acceptor molecules. If the wavelength λ is expressed in nanometers, then $J(\lambda)$ is in units of M^{-1} cm^{-1} nm^4 and the Förster critical radius, R_0 in angstroms (Å), is expressed as follows (eq 3)

$$R_0 = 0.2108 \times [K^2 \times \Phi_D \times n_R{}^{-4} \times J(\lambda)]^{1/6} \quad (3)$$

where K^2 is the orientation factor for the emission and absorption dipoles and its value depends on their relative orientation, n_R is the refractive index of the medium, and Φ_D is the quantum yield of the donor. $J(\lambda)$ is the overlap integral of the fluorescence emission spectrum of the donor and the absorption spectrum of the acceptor (Figure S6), as expressed by eq 4

$$J(\lambda) = \int_0^\infty F_D(\lambda) \times \varepsilon_A(\lambda) \times \lambda^4 \times d\lambda \quad (4)$$

where $F_D(\lambda)$ is the fluorescence intensity of the donor in the absence of acceptor normalized so that $\int_0^\infty F_D(\lambda)\, d\lambda = 1$; $\varepsilon_A(\lambda)$ is molar extinction coefficient of the acceptor, and λ is wavelength. In the current experimental conditions, for the nanoparticle-based sensor, $J(\lambda)$ was calculated to be 7.99×10^{13} M^{-1} cm^{-1} nm^4. The Förster critical radius (R_0) has been calculated as 30.8 Å, assuming random orientation of the donor and acceptor moieties taking $K^2 = 2/3$, $n_R = 1.49$ (PMMA), and $\Phi_D = 0.9$.

For this FRET-based sensing system with the polymeric nanoparticle as the scaffold, the NBD molecules (donors) reside in the particle core while the ring-opened rhodamine/Hg^{2+} complexes (acceptors) reside on the surface, and the effective energy transfer distance is from 1.54 nm (0.5 R_0) to 4.62 nm (1.5 R_0). Thus, for the nanoparticles, an outer sphere of about 4.62 nm thick can serve as the effective volume in which the excited-state energy of NBD can be transferred to the acceptor, as illustrated in Scheme S2 in the Supporting Information.

To compare the effect of particle size on the energy transfer efficiency, we listed the experimental energy transfer efficiency and the ratio of effective energy transfer volume to overall particle volume (V_e) for two nanoparticle samples in Table 1. For this FRET system, the effective energy transfer distance is generally less than 4.62 nm. For this particle-based FRET system whose radius is larger than the maximum effective energy transfer distance, the donors (NBD dye) distribute throughout the PMMA core and the acceptors reside at the particle surface. The FRET systems constructed in smaller particles have higher proportion of donors which can be quenched by the acceptors on the particle surface because of the limited energy transfer distance. Also, it can be seen that the smaller particle (NP40) exhibits higher V_e as well as higher E_m values. In this study, the

dx.doi.org/10.1021/jp109594h |J. Phys. Chem. B 2011, 115, 874–882

smallest size of the particle we can obtain by miniemulsion polymerization is around 40 nm in diameter (NP40), and we found the polymeric particle samples with their diameter higher than 60 nm are not suitable for accurate ratiometric sensing because the variation range for NBD's emission intensity is too narrow for the accurate calculation of a series of I_{595}/I_{505} values.

Moreover, the measured energy transfer efficiencies E_m for the two samples are fairly close to the calculated V_e values obtained from the Förster critical radius R_0, suggesting that most of donors in the effective energy transfer volume participated in the FRET process. Previously, we have constructed a FRET-based fluorescence modulation system in polymeric colloids prepared via heterogeneous nucleation emulsion polymerization or via atomic transfer radical polymerization (ATRP), and we found the calculated V_e values are far different from the measured energy transfer efficiency values.[57,60] The possible reason, we think, is that the miniemulsion polymerization can make the NBD molecules rather uniformly distribute within the nanoparticles, and the most NBD dyes (donor) in the effective volume of the nanoparticles can transfer their excited-state energy to the acceptors. According to the determined concentration for the donor and acceptor in the particle dispersion, the ratio of the number of SRHB (precursor of the acceptor) to donor is estimated as about 39 in the nanoparticles of the sample NP40, indicating this particle-based FRET system corresponds to a configuration where a single donor interacts with multiple acceptors, somewhat like the quantum dot-based FRET systems.[33] We found for this FRET system, a higher acceptor to donor ratio is needed to ensure the accurate ratiometric detection within a wider detection range (from 100 nM to 50 μM). The donor NBD dye exhibits very high quantum yield ($\sim$ 0.9) in the hydrophobic particle cores, and in the case of lower acceptor to donor ratio (less than 20), the fluorescence intensity for the acceptor became very low compared with the intensity of the donor at low concentration of Hg^{2+} (1 μM or below); this can reduce the accuracy of the ratiometric detection because the error for the measured intensity of the acceptor could be large at low ion concentration. Previously, we also found that in the micelle-based FRET system for ferric ion detection, the ratio of acceptor to donor had to be maintained high to achieve a wider range of ratiometric detection.[57]

3.5. Selectivity and pH Range for Hg^{2+} Sensing in Water. Figure 7 shows the fluorescence intensity ratio (I_{593}/I_{505}) of nanoparticle dispersion in the presence of different metal ions at pH 7.0. It is clear that the nanoparticle dispersion exhibits little fluorescence intensity change upon addition of 50 μM of metal ions such as K^+, Na^+, Ca^{2+}, Mg^{2+}, Al^{3+}, Zn^{2+}, Fe^{3+}, Mn^{2+}, Pb^{2+}, Cu^{2+}, Co^{2+}, Ni^{2+}, or Cr^{3+}; and only a slight increase in I_{593}/I_{505} was observed upon addition of 50 μM of Ag^+. On the other hand, addition of Hg^{2+} resulted in a prominent enhancement of fluorescence intensity ratio, indicating the nanoparticle system exhibits high selectivity for the detection of Hg^{2+} in water dispersion.

The effects of the coexisting ions for nanoparticle dispersion on mercury ion detection were also investigated, and the result was depicted in Figure 7b. It can be seen that most coexisting ions have negligible effect on the ratiometric detection for Hg^{2+}; only Cu^{2+} and Ag^+ can cause slight change in fluorescence intensity ratio. The result suggests that the coexistence of most selected metal ions does not interfere with the complexation of Hg^{2+} with the spirolactam rhodamine probe and the subsequent fluorescence turn-on.

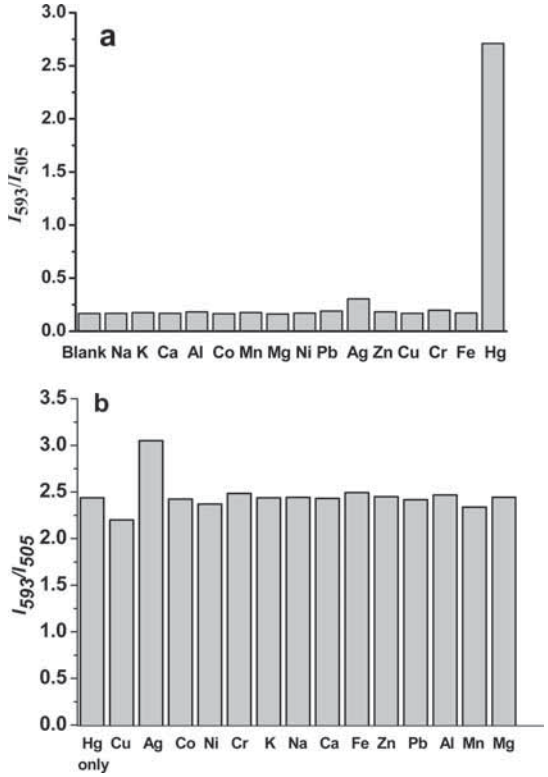

Figure 7. (a) Fluorescence intensity ratio (I_{593}/I_{505}) of nanoparticle dispersion upon addition of different metal ions (50 μM), respectively. (b) Fluorescence intensity ratio (I_{593}/I_{505}) of nanoparticle dispersion in the presence of 40 μM of Hg^{2+} with 40 μM of various coexisting metal cations respectively. Hg^{2+} only: in the presence of 40 μM of Hg^{2+} only. (λ_{exc}: 420 nm, pH 7.0, HEPES.)

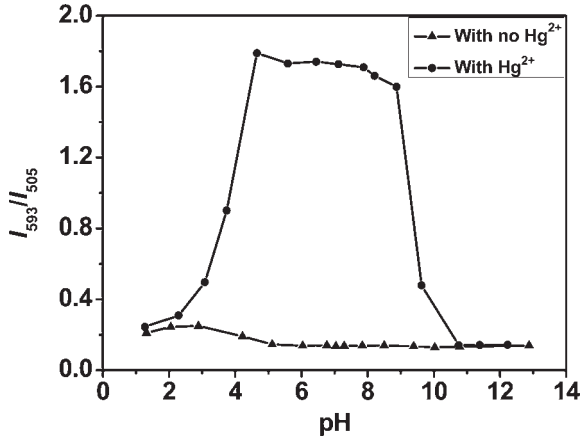

Figure 8. Variation of I_{593}/I_{505} for the NP40 nanoparticle dispersion with and without the presence of Hg^{2+} (25 μM) as a function of pH (λ_{exc}: 420 nm).

For practical applicability, we also investigated the suitable pH range for mercury ion sensing. The effect of pH on the fluorescence ratio of the nanoparticle dispersion is given in Figure 8. In the absence of Hg^{2+}, the rhodamine B moieties on the nanoparticles remained the spirolactam structure, and no remarkable fluorescence emission was observed in the pH range from 2 to13, suggesting that the nanoparticle dispersion is stable

over a wide pH range. In the presence of Hg^{2+}, a remarkable increase in fluorescence intensity ratio was observed between pH 4 and 9, indicating in this pH range the mercury ions can cause the ring-opening of the spirolactam rhodamine. It also can be found that the dispersion exhibits high fluorescence intensity ratios which remained fairly stable from pH 4 to pH 8. These data establish that the polymeric nanoparticle dispersion could serve as a ratiometric fluorescent sensor for Hg^{2+} under physiological pH conditions.

4. CONCLUSIONS

In summary, we have developed a FRET-based ratiometric sensing system with polymeric nanoparticle as the scaffold for detecting Hg^{2+} via miniemulsion polymerization. By embedding the donor in the particle core and covalently linking the mercury ion recognition probe on the surface, we successfully obtained a FRET system within individual particles which are capable of detecting Hg^{2+} sensitively and selectively. The FRET process within the individual nanoparticles not only allows for ratiometric sensing of Hg^{2+} but also realized a large shift (>170 nm) between donor excitation and acceptor emission, which rules out any influence of excitation backscattering effects on fluorescence detection. This strategy could provide a new approach for ratiometric detecting of mercury ion in environmental and biological applications and could be applied to construct other rhodamine-based sensors for other metal ion detection.

■ ASSOCIATED CONTENT

Supporting Information. Characterizations, schemes, absorption and fluorescence spectra, and photographs. This material is available free of charge via the Internet at http://pubs.acs.org.

■ AUTHOR INFORMATION

Corresponding Author

*E-mail: shzhwu@scut.edu.cn (S.W.), mcfzeng@scut.edu.cn (F.Z.); phone (+86)-20-22236262; fax (+86)-20-22236363.

■ ACKNOWLEDGMENT

This work was supported by NSFC (Project Nos. 21025415, 20974035, and 50973032) and by "the Fundamental Research Funds for the Central Universities, SCUT".

■ REFERENCES

(1) Nendza, M.; Herbst, T.; Kussatz, C.; Gies, A. *Chemosphere* **1997**, *35*, 1875–1885.
(2) Wang, Q.; Kim, D.; Dionysiou, D. D.; Sorial, G. A.; Timberlake, D. *Environ. Pollut.* **2004**, *131*, 323–336.
(3) Homma-Takeda, S.; Shinyashiki, M.; Kumagai, Y.; Shimojo, N. J. *Occup. Health* **1996**, *38*, 118–119.
(4) Clarkson, T. W.; Magos, L.; Myers, G. J. *Engl. J. Med.* **2003**, *349*, 1731–1737.
(5) Guo, T.; Baasner, J.; Gradl, M.; Kistner, A. *Anal. Chim. Acta* **1996**, *320*, 171–176.
(6) Bloom, N.; Fitzgerald, W. F. *Anal. Chim. Acta* **1988**, *208*, 151–161.
(7) *Method 1631 Revision B: Mercury in Water by Oxidation, Purge and Trap, and Cold Vapor Atomic Fluorescence Spectrometry*; EPA-821-R-99-005; EPA Office of Water: Washington, DC, May 1999.
(8) Fitzgerald, W. F.; Gill, G. A. *Anal. Chem.* **1979**, *51*, 1714–1720.
(9) Rosi, N. L.; Mirkin, C. A. *Chem. Rev.* **2005**, *105*, 1547–62.
(10) Nolan, E.M .; Lippard, S. *J. Chem. Rev.* **2008**, *108*, 3443–80.
(11) Liu, X.; Zhu, J. *J. Phys. Chem. B* **2010**, *113*, 8214–8217.
(12) Burress, C. N.; Bodine, M. I.; Elbjeirami, O.; Reibenspies, J. H.; Omary, M. A.; Gabbai, F. P. *Inorg. Chem.* **2007**, *46*, 1388–1395.
(13) Zhu, X.; Fu, S.; Guo, J.; Wong, W. *Angew. Chem., Int. Ed.* **2006**, *45*, 3150–3154.
(14) Yang, Y.; Gou, X.; Blecha, J. *Tetrahedron Lett.* **2010**, *51*, 3422–3425.
(15) Martinez, R.; Espinosa, A.; Tarraga, A. *Tetrahedron.* **2010**, *66*, 3662–3667.
(16) Kim, H. N.; Lee, M. H.; Kim, H. J.; Kim, J. S.; Yoon, J. *Chem. Soc. Rev.* **2008**, *37*, 1465–1472.
(17) Tsien, R. Y.; Poenie, M. *Trends Biochem. Sci.* **1986**, *11*, 450–455.
(18) Kubo, Y.; Yamamoto, M.; Ikeda, M.; Takeuchi, M.; Shinkai, S.; Yamaguchi, S.; Tamao, K. *Angew. Chem., Int. Ed.* **2003**, *42*, 2036–2040.
(19) Ajayaghosh, A.; Carol, P.; Sreejith, S. *J. Am. Chem. Soc.* **2005**, *127*, 14962–14963.
(20) Zhou, Y.; Zhu, C. Y.; Gao, X. S.; You, X. Y.; Yao, C. *Org. Lett.* **2010**, *12*, 2566–2569.
(21) Kim, S. K.; Swamy, K.; Chung, S. Y.; Kim, H. N.; Kim, M. J.; Jeong, Y.; Yoon, J. *Tetrahedron Lett.* **2010**, *51*, 3286–3289.
(22) Liu, H. Z.; Yu, P.; Du, D.; He, C. Y.; Qiu, B.; Chen, X.; Chen, G. A. *Talanta* **2010**, *81*, 433–437.
(23) Suresh, M.; Mishra, S.; Mishra, S. K.; Suresh, E.; Mandal, A. K.; Shrivastav, A.; Das, A. *Org. Lett.* **2009**, *11*, 2740–2743.
(24) Joshi, B. P.; Park, J.; Lee, W. I.; Lee, K. H. *Talanta* **2009**, *78*, 903–909.
(25) Zhang, X. L.; Xiao, Y.; Qian, X. H. *Angew. Chem., Int. Ed.* **2008**, *47*, 8025–8029.
(26) Ueyama, H.; Takagi, M.; Takenaka, S. *J. Am. Chem. Soc.* **2002**, *124*, 14286–14287.
(27) Shang, G. Q.; Gao, X.; Zheng, H. *J Fluoresc.* **2008**, *18*, 1187–1192.
(28) Lakowicz, J. R. *Principles of Fluorescence Spectroscopy*; Plenum: New York, 1999.
(29) Medintz, I. L.; Pons, T.; Susumu, K.; Boeneman, K.; Dennis, A. M.; Farrell, D.; Deschamps, J. R.; Melinger, J. S.; Bao, G.; Mattoussi, H. *J. Phys. Chem. C* **2009**, *113*, 18552–18561.
(30) Lovell, J. F.; Chen, J.; Jarvi, M. T.; Cao, W. G.; Allen, A. D.; Liu, Y.; Tidwell, T. T.; Wilson, B. C.; Zheng, G. *J. Phys. Chem. B* **2009**, *113*, 3203–3211.
(31) Mountford, C. P.; Buck, A. H.; Campbell, C. J.; Dickinson, P.; Ferapontova, E. E.; Terry, J. G.; Beattie, J. S.; Walton, A. J.; Ghazal, P.; Mount, A. R.; Crain, J. *J. Phys. Chem. B* **2008**, *112*, 2439–2444.
(32) Wu, S.; Luo, Y.; Zeng, F.; Chen, J.; Tong, Z. *Angew. Chem., Int. Ed.* **2007**, *46*, 7015–7018.
(33) Clap, A. R.; Medintz, I. L.; Mattoussi, H. *Phys. Chem. Chem. Phys.* **2006**, *7*, 47–57.
(34) Pons, T.; Medintz, I. L.; Sapsford, K. E.; Higashiya, S.; Grimes, A. F.; English, D. S.; Mattoussi, H. *Nano Lett.* **2007**, *7*, 3157–3164.
(35) Pons, T; Medintz, I. L.; Wang, X.; Mattoussi, H. *J. Am. Chem. Soc.* **2006**, *128*, 15324–15331.
(36) Medintz, I. L.; Sapsford, K. E.; Clapp, A. R.; Pons, T.; Higashiya, S.; Welch, J. T.; Mattoussi, H. *J. Phys. Chem. B* **2006**, *110*, 10683–10690.
(37) Medintz, I. L.; Trammell, S. A.; Mattoussi, H.; Mauro, J. M. *J. Am. Chem. Soc.* **2004**, *126*, 30–31.
(38) Tomasulo, M.; Giordani, S.; Raymo, F. *Adv. Funct. Mater.* **2005**, *15*, 787–794.
(39) Yildiz, I.; Gao, X.; Harris, T. K.; Raymo, F. *J. Biomed. Biotechnol.* **2007**, 18081.
(40) Raymo, F. M.; Toasulo, M. *J. Phys. Chem. A* **2005**, *109*, 7343–7352.
(41) Ghadiali, J. E.; Cohen, B. E.; Stevens, M. M. *Nano* **2010**, *4*, 4915–4919.
(42) Deng, C. Y.; Li, J. M.; Ma, W. Y. *Talanta* **2010**, *82*, 771–774.
(43) Buranda, T.; Wu, Y.; Perez, D.; Chigaev, A.; Sklar, L. A. *J. Phys. Chem. B* **2010**, *114*, 1336–1349.

(44) Xu, C. S.; Kim, H.; Hayden, C. C.; Yang, H. *J. Phys. Chem. B* **2010**, *114*, 5917–5923.
(45) Sarkar, R.; Narayanan, S. S.; Palsson, L. O.; Dias, F.; Monkman, A.; Pal, S. K. *J. Phys. Chem. B* **2007**, *111*, 12294–12298.
(46) Tang, Z. Y.; Ozturk, B.; Wang, Y.; Kotov, N. A. *J. Phys. Chem. B* **2004**, *108*, 6927–6931.
(47) Haldar, K. K.; Sen, T.; Patra, A. *J. Phys. Chem. C* **2010**, *114*, 4869–4874.
(48) Sadhu, S.; Haldar, K. K.; Patra, A. *J. Phys. Chem. C* **2010**, *114*, 3891–3897.
(49) Curutchet, C.; Franceschetti, A.; Zunger, A.; Scholes, G. D. *J. Phys. Chem. C* **2008**, *112*, 13336–13341.
(50) Brasola, E.; Mancin, F.; Rampazzo, E.; Tecilla, P.; Tonellato, U. *Chem. Commun.* **2003**, 3026–3027.
(51) Marcon, L.; Spriet, C.; Meehan, T. D.; Battersby, B. J.; Lawrie, G. A.; Heliot, L.; Trau, M. *Small* **2009**, *5*, 2053–2056.
(52) Kim, S. H.; Jeyakumar, M.; Katzenellenbogen, J. A. *J. Am. Chem. Soc.* **2007**, *129*, 13254–13264.
(53) Zhu, M. Q.; Zhu, L.; Han, J. J.; Wu, W.; Hurst, J. K.; Li, A. D. Q. *J. Am. Chem. Soc.* **2006**, *128*, 4303–4309.
(54) Zhu, L. Y.; Wu, W. W.; Zhu, M. Q.; Han, J. J.; Hurst, J. K.; Li, A. D. Q. *J. Am. Chem. Soc.* **2007**, *129*, 3524–3526.
(55) Gouanve, F.; Schuster, T.; Allard, E.; Meallet-Renault, R.; Larpent, C. *Adv. Funct. Mater.* **2007**, *17*, 2746–2756.
(56) Chen, J.; Zeng, F.; Wu, S.; Chen, Q.; Tong, Z. *Chem.—Eur. J.* **2008**, *14*, 4851–4860.
(57) Ma, B.; Wu, S.; Zeng, F.; Luo, Y.; Zhao, J.; Tong, Z. *Nanotechnology* **2010**, *21*, 195501.
(58) Chen, J.; Zeng, F.; Wu, S; Su, J.; Tong, Z. *Small* **2009**, *5*, 970–978.
(59) Chen, J.; Zeng, F.; Wu, S.; Zhao, J; Chen, Q.; Tong, Z. *Chem. Commun.* **2008**, 5580–5582.
(60) Chen, J.; Zeng, F.; Wu, S. *Chem. Phys. Chem* **2010**, *11*, 1036–1043.
(61) Jones, C. D.; McGrath, J. G.; Lyon, L. A. *J. Phys. Chem. B* **2004**, *108*, 12652–12657.
(62) Lee, J.; Kim, H. J.; Chen, T.; Kotov, N. A. *J. Phys. Chem. C* **2009**, *113*, 109–116.
(63) Prazeres, T.; Farinha, J.; Martinho, J. *J. Phys. Chem. C* **2008**, *112*, 16331–16339.
(64) Li, C. H.; Zhang, Y. X.; Hu, J. M.; Cheng, J. J.; Liu, S. Y. *Angew. Chem., Int. Ed.* **2010**, *49*, 5120–5124.
(65) Hu, J. M.; Li, C. H.; Liu, S. Y. *Langmuir* **2010**, *26*, 724–729.
(66) Wu, T.; Zhang, Y. F.; Wang, X. F.; Liu, S. Y. *Chem. Mater.* **2008**, *20*, 101–109.
(67) Valeur, B. *Molecular Fluorescence: Principles and Applications*; Wiley-VCH: New York, 2002.
(68) Asua, J. M. *Prog. Polym. Sci.* **2002**, *27*, 1283.
(69) Landfester, K.; Schork, F. J.; Kusuma, V. A. *C. R. Chim.* **2003**, *6*, 1337–1342.
(70) Antonietti, M.; Landfester, K. *Prog. Polym. Sci.* **2002**, *27*, 689–757.
(71) Ramirez, L. P.; Landfester, K. *Macromol. Chem. Phys.* **2003**, *204*, 22–31.
(72) Holzapfel, V.; Lorenz, M.; Weiss, C. K.; Schrezenmeier, H.; Landfester, K.; Mailander, V. *J. Phys.: Condens. Matter* **2006**, *18*, S2581–2594.
(73) Takasu, M.; Shiroya, T.; Takeshita, K.; Sakamoto, M.; Kawaguchi, H. *Colloid Polym. Sci.* **2003**, *282*, 119–126.
(74) Ando, K.; Kawaguchi, H. *J. Colloid Interface Sci.* **2005**, *285*, 619–626.
(75) Tamai, T.; Watanabe, M.; Maeda, H.; Mizuno, K. *J. Polym. Sci., Part A: Polym. Chem.* **2008**, *46*, 1470–1475.
(76) Tu, C. F.; Yang, Y. H.; Gao, M. Y. *Nanotechnology* **2008**, *19*, 105601.
(77) Han, M.; Lee, E.; Kim, E. *Opt. Mater.* **2003**, *21*, 579–583.
(78) Zheng, H.; Qian, Z.; Xu, L.; Yuan, F.; Lan, L.; Xu, J. *Org. Lett.* **2006**, *8*, 859–861.